In situ observations of crack propagation and role of grain boundary microstructure in nickel embrittled by sulfur

Shigeaki Kobayashi, Tatsuya Maruyama, Sakae Saito, Sadahiro Tsurekawa & Tadao Watanabe

Journal of Materials Science
Full Set - Includes `Journal of Materials Science Letters'

ISSN 0022-2461
Volume 49
Number 11

J Mater Sci (2014) 49:4007-4017
DOI 10.1007/s10853-014-8056-z

Springer

J Mater Sci (2014) 49:4007–4017
DOI 10.1007/s10853-014-8056-z

INTERGRANULAR AND INTERPHASE BOUNDARIES

In situ observations of crack propagation and role of grain boundary microstructure in nickel embrittled by sulfur

Shigeaki Kobayashi · Tatsuya Maruyama · Sakae Saito · Sadahiro Tsurekawa · Tadao Watanabe

Received: 24 September 2013 / Accepted: 15 January 2014 / Published online: 28 January 2014

Abstract In situ observations of crack propagation in sulfur-doped coarse-grained nickel were performed for the specimens with grain boundary microstructure pre-determined by SEM/EBSD analysis. The role of grain boundary microstructure was studied in the crack propagation in nickel embrittled by grain boundary segregation of sulfur. It was found that the main crack tends to predominantly propagate along random boundaries, and the crack propagation rate can be locally accelerated at the grain boundary network with a high connectivity of random boundaries. On the other hand, the cracks can propagated along fracture-resistant low-Σ coincidence site lattice (CSL) boundary only when the trace of the grain boundary is arranged being almost parallel to slip bands in the adjacent grains. The local crack propagation rate was found to become lower when a crack propagated along low-Σ CSL boundaries. Moreover, when the crack propagation is inhibited by low-Σ CSL boundaries, the branching of propagating crack occurs at partially cracked triple junctions. The crack propagation can locally slow down due to the occurrence of crack branching. The optimum grain boundary microstructure for the control of sulfur segregation-induced brittle fracture is discussed on the basis of new findings obtained from the in situ observations on crack propagation and fracture processes in polycrystalline nickel.

S. Kobayashi (✉) · T. Maruyama · S. Saito
Division of Mechanical and Electrical Engineering, Department of Innovative Engineering, Faculty of Engineering, Ashikaga Institute of Technology, 268-1 Omae, Ashikaga, Tochigi 326-8558, Japan
e-mail: skoba@ashitech.ac.jp

S. Tsurekawa
Department of Materials Science and Engineering, Graduate School of Science and Technology, Kumamoto University, Kumamoto 860-8555, Japan

T. Watanabe
Key Laboratory for Anisotropy and Texture of Materials, Northeastern University, Shenyang 110004, China

T. Watanabe
Tohoku University, Sendai, Japan

Introduction

Grain boundary fragility due to grain boundary segregation of solute or impurity atoms in engineering materials has been extensively studied and discussed since early time of the history of grain boundary research [1]. It is well known that grain boundary segregation of sulfur atoms causes severe embrittlement and degradation of performance reliability in polycrystalline nickel-based alloys which are used as high temperature structural materials [2–4]. Quantitative experimental works of grain boundary segregation in metallic materials have been performed previously, particularly using Auger electron spectroscopy (AES) analysis since 1980s [5–7]. It has been revealed that the degree of grain boundary segregation of detrimental elements at specific grain boundaries strongly depends on the grain boundary character and structure in some alloy systems such as Fe–Sn alloy [5, 6], Fe–Si alloy [7] and other metallic materials, as fully discussed in the most recent book on grain boundary segregation by Lejček [8]. This has been confirmed by experiments for grain boundary segregation of sulfur in nickel [9, 10]. It has been reported that the degree of segregation of sulfur at special (low-energy) boundaries tends to be lower than that at general (high-energy) boundaries for the nickel-sulfur system [10]. Moreover, the resistance to segregation-induced intergranular fracture at low-Σ coincidence site lattice (CSL) boundaries with lower energy was found to be higher than those at random high-energy boundaries [11–15]. Therefore, the grain boundary segregation-induced embrittlement in polycrystalline materials can be controlled by grain boundary engineering (GBE) by manipulating at least "grain boundary character distribution (GBCD)" and "grain boundary connectivity", as documented in recent reviews on the GBE [16, 17].

The usefulness of GBE for control of grain boundary degradation phenomena such as intergranular corrosion has been proved by many researchers [18–22], and discussed in recent Watanabe's review on GBE [17]. However, unfortunately, such a promising application of the GBE for control of segregation-induced embrittlement has been not much attempted so far [23–26]. Quite recently, the present authors have revealed that the fracture toughness of sulfur-doped ultrafine-grained nickel specimens produced by electrodeposition and subsequent annealing is strongly influenced by the fraction of low-Σ CSL boundaries [25]. Furthermore, we have investigated the effect of grain boundary microstructure on the fracture resistance of sulfur-doped ordinary polycrystalline nickel, in order to establish the utility of GBE for the control of segregation-induced embrittlement in polycrystalline materials [26]. In the course of the previous studies, we have introduced a new grain boundary microstructural parameter that can quantitatively describe the connectivity of fracture susceptive random boundaries on the basis of fractal analysis. We have found that the random boundary network with maximum connectivity (maximum random boundary connectivity, MRBC) is of fractal nature reflecting the distributions of a large variety of grain size and grain shape. It has been revealed that the fractal dimension of MRBC can be effectively used to predict and control the fracture resistance and intergranular brittleness in polycrystalline nickel embrittled by grain boundary segregation of sulfur [26]. However, these findings for the fracture processes in sulfur-doped nickel must be confirmed further by experiment, if possible, through in situ direct observations of the crack propagation, which is the percolation process in grain boundary network, probably affected by the GBCD and grain boundary connectivity associated with the spatial distribution of high-energy random boundaries or low-energy specific grain boundaries.

In the present work, in situ observations of crack propagation were performed for the sulfur-doped polycrystalline nickel in which individual grain boundaries were characterized using the field emission gun-scanning electron microscopy (FEG-SEM)/electron backscattered diffraction (EBSD)/orientation imaging microscopy (OIM), in order to reveal the roles of grain boundary microstructure in crack propagation processes in nickel embrittled by sulfur segregation. The roles of different types of grain boundaries and triple junctions in crack deflection and branching were investigated in focusing our attention to the variety of nature of the grain boundary network in polycrystals. Of particular interest was the effect of the grain boundary connectivity on the local propagation rate of cracks in fracture processes of grain boundary network. The importance of grain boundary microstructure for the control of segregation-induced intergranular fracture in polycrystalline materials is discussed on the basis of new findings obtained from in situ observations in nickel.

Experimental procedure

Specimen preparation

A fully annealed polycrystalline nickel sheet with the purity of 99.75 % was subjected to cold rolling to 75 % in reduction ratio and subsequent annealing at 1273 K (0.74 T_m, T_m is a melting point of nickel) for 10.8 ks. The specimen and sulfur powders (0.04 g) were enclosed together in a Pyrex glass tube with 8 mm internal diameter and 70 mm length in a vacuum of 3×10^{-3} Pa. Sulfur powders were put in an aluminum foil boat, to prevent the nickel specimen from direct contact with sulfur powders. They were heated at 873 K (0.51 T_m) for 72 h. This heat treatment could introduce the sulfur content of 290 ppm into the nickel specimen. The equilibrium sulfur content at grain boundaries was roughly estimated to be 95 at% using the Langmuir-McLean equation [8]. However, it is very likely that the condition of sulfur-doping heat treatment carried out in the present work might not be sufficient to reach the equilibrium state. Using Auger electron spectroscopy (AES), Loier and Boos [4] have determined and reported that the nickel specimens with the bulk sulfur concentration of 70 and 100 ppm possessed the intergranular sulfur concentration of 10.0 and 14.5 at%, respectively, even after heating at 1473 K for 20 days. Therefore, the level of the grin boundary sulfur concentration should be at least more than 10.0 at% order, when polycrystalline nickel specimens with sulfur exhibit sulfur-induced intergranular fracture. Moreover, as simply predicted by the Seah-Hondros diagram for the Ni–S system, it is very likely that the presence of sulfide phase (such as Ni_3S_2 with low-melting temperature) at grain boundaries can enhance intergranular fracture [27].

The single-edge-notched specimens whose dimensions were 40.0 mm length, 4.0 mm wide and 3.0 mm thick were cut out by a spark machine from the heat treated sheet for crack propagation test. A notch with 0.3 mm wide and 0.5 mm depth was introduced at the center of the longitudinal direction of the specimen. In order to characterize the grain boundary microstructure by SEM/EBSD analyses, the surface of the specimens was mechanically polished using emery papers of 320–1000 grade and 0.06 μm alumina powder slurry. Then specimen surfaces were electrolytically polished in an electrolytic solution of 79 vol% acetic acid, 15 vol% methanol, and 6 vol% perchloric acid at a current density of 4.0 mA/mm^2 at 280 K for 20 s. Finally, they were weakly etched using a solution of 50 vol% acetic acid and 50 vol% nitric acid at room temperature for 3 s, to reveal the grain boundary configuration.

Characterization of grain boundary microstructure

The grain boundary microstructure in the studied sulfur-doped nickel specimens was quantitatively characterized using FE-SEM/EBSD/OIM system. Based on the relative orientation relationship and the misorientation angle between adjoining grains, individual grain boundaries are conventionally defined as low-angle ($\theta < 15^{\circ}$, $\Sigma 1$), high-angle special/low-Σ ($3 \leq \Sigma \leq 29$) CSL boundaries, and high-angle general/random boundaries ($\theta > 15^{\circ}$, without any CSL relationship), based on coincidence lattice site relationship [28], under the Brandon's criterion, $\Delta\theta = 15/\Sigma^{1/2}$ [29]. We have already obtained much experimental evidence for the finding that low-Σ CSL boundaries ($\Sigma < 29$) show special properties which are never observed for random boundaries, although, strictly speaking, the grain boundary character is not fully defined by the relative orientation relationship and Σ-value. We need some information on the grain boundary plane. However, the effectiveness of GBCD evaluated by the conventional characterization method of grain boundary microstructure has been well proved in recent attempts of GBE for fracture control and high performance [30–33].

In situ observations of fatigue crack propagation in sulfur-doped nickel specimens

Crack propagation tests under cyclic loading were carried out using a servo-hydraulic machine (Shimadzu, Servo-pulser). Four-point bending load was cyclically applied to the sulfur-doped nickel specimens. The gauge distances of the four-point bending jig were 30 mm between the outer supporting pins and 10 mm between the inner loading pins. Sinusoidal load was applied in air at room temperature, at a constant load amplitude (31.5 N), load ratio (0.1), and frequency (5 Hz).

In situ observations of crack propagation processes (intergranular fracture and/or transgranular fracture) were made using the 2D-motion capture system (Detect, Motion-Pro) consisting of a CCD camera mounting a high magnification/long focal distance lens and a computer with an A/D converter and a video capture card. A schematic illustration of this observation system is shown in Fig. 1.

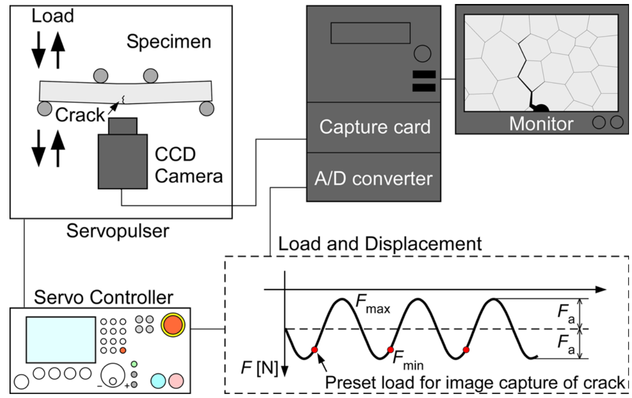

Fig. 1 Schematic illustration of the experimental set-up used for in situ observation of crack propagation during cyclic bending test

The observed images of cracks during cyclic loading were captured in the computer at a regular cycle interval via CCD camera and video capture card, only when the sinusoidal load reached to a preset value. Every step of crack propagation was captured and evaluated in connection with the characteristic features of grain boundary microstructures determined for each specimen prior to fracture test under cyclic loading.

Results and discussion

Grain boundary microstructures of sulfur-doped nickel specimen

Figure 2a–c shows the grain boundary micrograph, the grain size distribution, the inverse pole figure with GBCD data for the sulfur-doped nickel specimen, respectively. In the grain boundary micrograph, Fig. 2a, the types of grain boundaries are shown by distinct colors corresponding to those indicated in the color bars on the right-hand side of the micrograph. For example, low-angle ($\Sigma 1$), $\Sigma 3$ CSL boundaries, and random boundaries are shown by red, green and black lines, respectively. It was found that the sulfur-doped nickel specimen had coarse-grained structure and contained a large number of annealing twins bordered by coherent $\Sigma 3$ boundaries, typically for nickel with middle level of stacking fault energy (128×10^{-3} J/mm^2 [34]).

As shown in Fig. 2b, the grain size distribution of the sulfur-doped nickel specimen ranged from 20 to 320 μm. An average grain size of the specimen was 84.4 μm so that some 35 grains might be connected in the specimen thickness.

The surface orientation of tested nickel specimens appeared to orient toward {001} and {101} (Fig. 2c). As indicated by the attached table of GBCD, the total fraction of low-Σ CSL boundaries in this specimen was of 46 %,

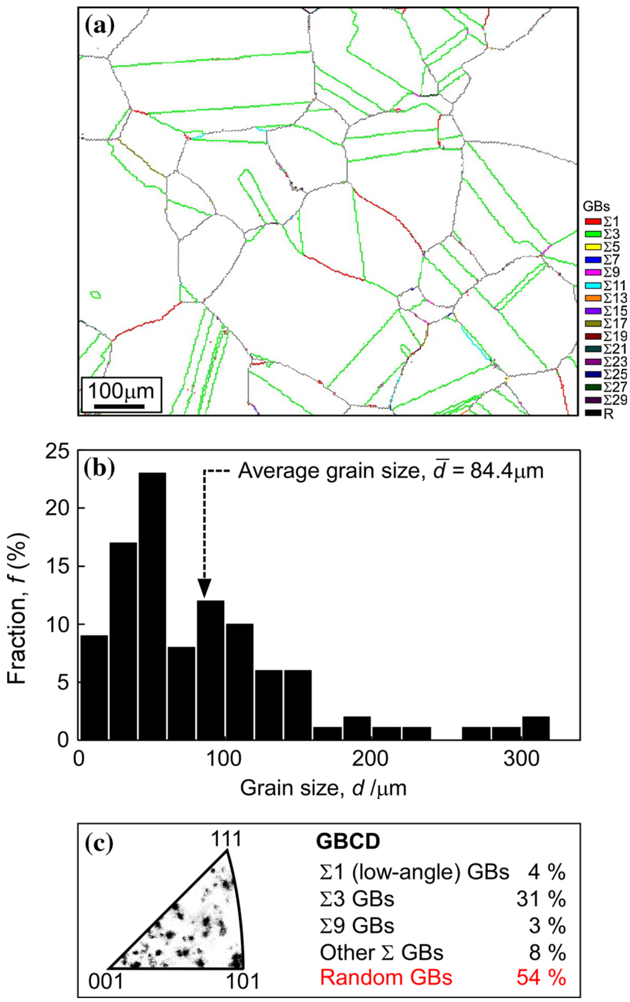

Fig. 2 **a** Grain boundary microstructure (GBM) map, **b** grain size distribution, **c** inverse pole figure with grain boundary character distribution (GBCD) data of pre-deformed sulfur-doped nickel specimen

and $\Sigma 3$ boundaries occupied a high fraction of 31 % of the total fraction. The occurrence of a high fraction of $\Sigma 3$ boundaries may be ascribed to the dominant evolution of annealing twins. In the present investigation, these {111} coherent annealing twin boundaries are hereafter classified as $\Sigma 3$ boundaries.

In situ observations of crack propagation processes in sulfur-doped polycrystalline nickel during cyclic loading

Figure 3a shows one of in situ observations on crack propagation processes in the sulfur-doped nickel specimen (Specimen-1) during cyclic loading. In this figure, the loading axis is horizontal direction. The character of individual grain boundaries surrounding the coarse grain in the center (with the grain diameter of almost 500 μm) is indicated by different symbols in the micrographs. Low-Σ CSL and random boundaries are denoted by Σ plus numeral and R, respectively. Low-angle boundaries are indicated as $\Sigma 1$ CSL boundaries. The pink lines show slip lines induced by cyclic loading. Figure 3b shows the observed change in local crack propagation rate for the Specimen-1 with the grain boundary microstructure already shown in Fig. 3a. Here, let us examine the observed individual crack paths indicated by different kinds of lines, such as solid line and dashed line, for the crack propagation processes in this specimen.

The pre-crack stayed at the triple junction T_1 where the three random boundaries interconnected (Fig. 3a/(i)). The crack advanced along two random boundaries from the triple junction T_1 toward the triple junction T_2 on the right-hand side during the numbers of cyclic loads N reach to 2000 cycles (Fig. 3a/(ii)). The average crack propagation rate in this period was 6.2×10^{-3} μm/cycle, as shown in Fig. 3b. The crack did not propagate toward the triple junction T_3 composed of $\Sigma 1$, $\Sigma 3$, and random boundaries on the left-hand side of the triple junction T_1. From our previous study on the triple junction hardening in intrinsically brittle molybdenum [35, 36], it was found that the triple junctions composed of more than two low-Σ CSL boundaries show higher fracture resistance. The stress concentration associated with dislocation pile-ups is suggested to be higher around the triple junctions with higher connectivity of low-Σ CSL boundaries, because of the more difficult accommodation of lattice dislocations at these low-energy CSL boundaries [37, 38]. Nevertheless, the crack tends to propagate selectively along the path with a higher connectivity of "intrinsically weak high-energy" random boundaries [32] toward the triple junction T_2, because the triple junction T_3 inhibited the crack propagation. The exactly same finding was already obtained from early in situ observations on crack propagation in Bi-doped coarse-grained copper [39].

As shown in Fig. 3a/(iii), the crack kept remaining at the triple junction T_2 where $\Sigma 1$ and random boundaries lying in the crack propagation direction, for further more than 1000 cycles up to $N = 3000$. Then slip lines were newly generated in the grains locating in front of the advancing crack tip, when the number of cyclic loading reached 5000 cycles (Fig. 3a/(iv)). Further extension of these slip lines was inhibited by the random boundary, R_1, which was almost aligned in the horizontal direction. The numbers of the slip lines tend to increase with increasing the number of cyclic loading (Fig. 3a/(iv–vi)). The crack advanced slowly along the random boundary R_1, resulting from the stress concentration caused by the interaction between lattice dislocations within slip lines and the random boundary R_1. The crack propagation was arrested by the triple junction T_4 where $\Sigma 1$ boundary laid in the crack propagation direction (Fig. 3a/(vii)). As shown in Fig. 3b, the crack propagation

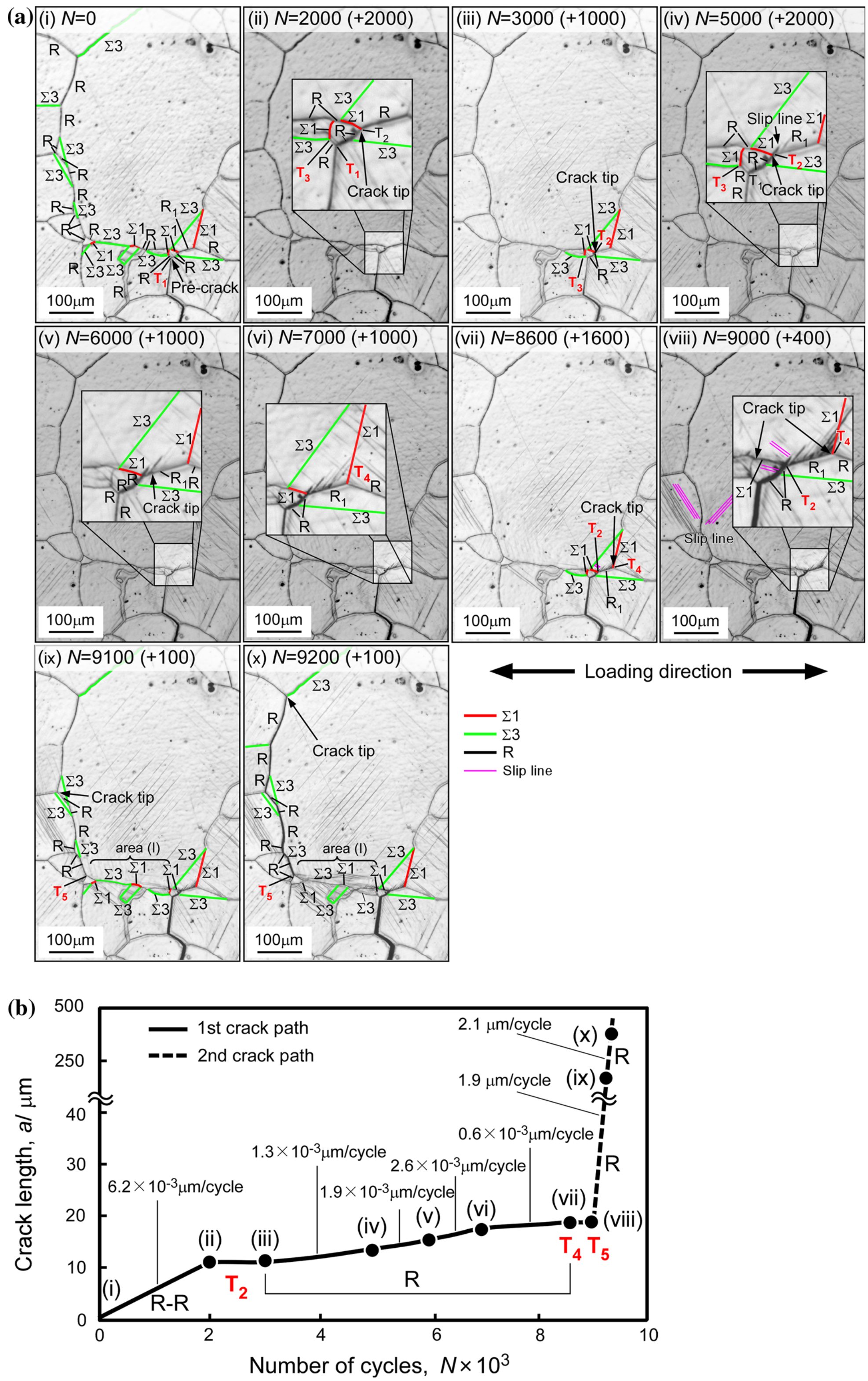

Fig. 3 **a** A bird's-eye view of intergranular crack propagation in the grain boundary network associated with heterogeneous grain structure, and **b** change in the local crack propagation rate in sulfur-doped nickel specimen A during cyclic bending test

was accelerated along the single random boundary (R_1) on the right-hand side of triple junction T_2 by development of slip lines, and then the propagation rate of crack gradually lowered, as it approached the triple junction T_4.

On the other hand, immediately after the stoppage of crack propagation occurred at the triple junction T_4, another crack propagation path occurred along the $\Sigma 1$ boundaries on the left-hand side of the triple junction T_2. As a result of this,

Fig. 4 **a** A bird's-eye view of crack propagation in the grain boundary network associated with homogeneous grain structure, and **b** change in the local crack propagation rate in sulfur-doped nickel specimen A during cyclic bending test. F_t is the propagation rate of transgranular crack

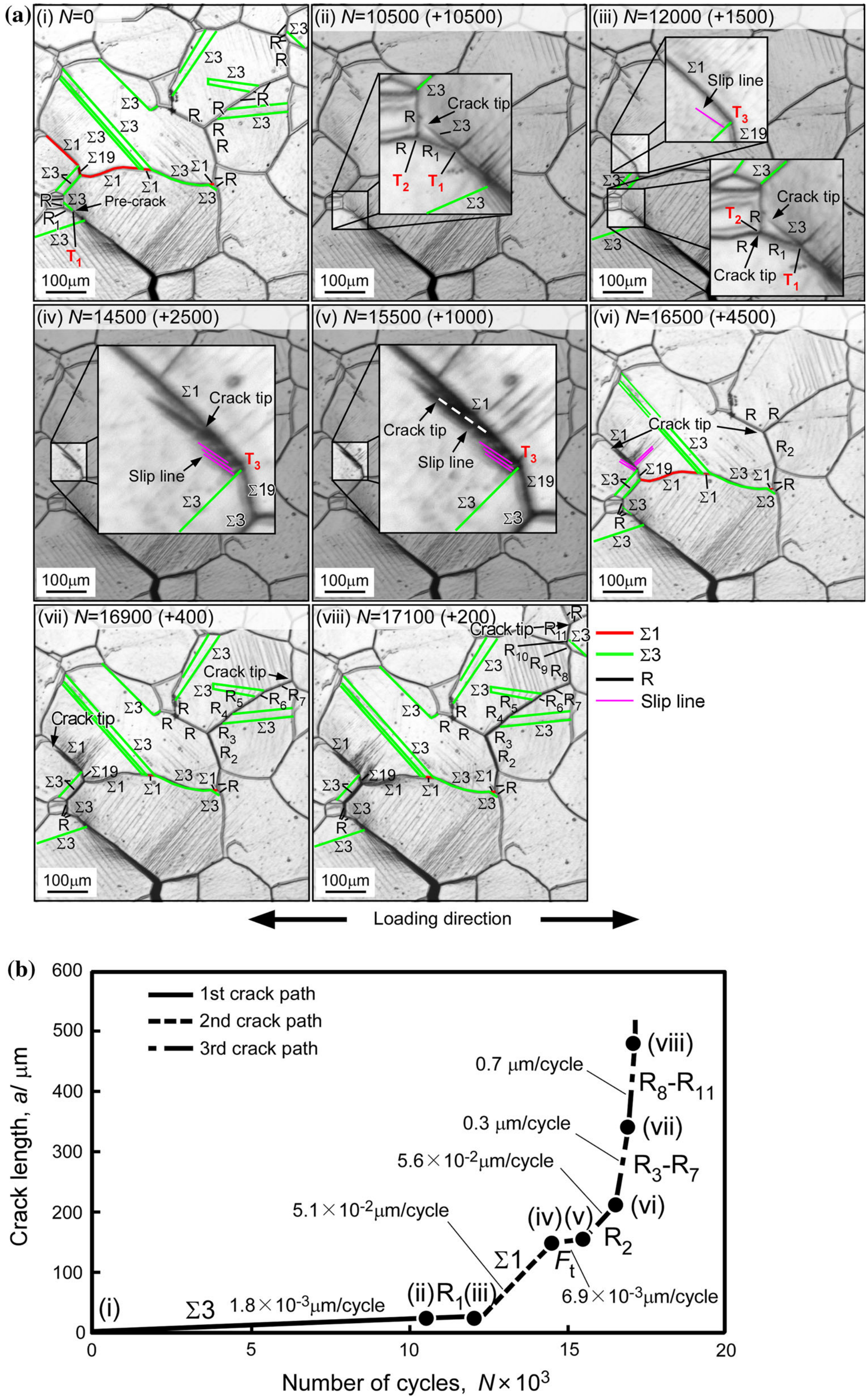

the branching of crack occurred at the triple junction T_2 after $N = 9000$, as seen from Fig. 3a/(viii). The slip bands almost parallel to the path of cracked $\Sigma 1$ boundary were observed in the adjacent grains. The more difficult cracking of the $\Sigma 1$ boundary than random boundary probably resulted from the heavy stress concentration produced by extensive interaction between the $\Sigma 1$ boundary and localized crystal slip during cyclic deformation (Fig. 3a/(viii)). Nevertheless, the crack propagation was completely stopped later on the $\Sigma 1$ boundary.

As for further stage of crack propagation, another crack path appeared around the triple junction T_5, on the left-hand area, after the stoppage of crack propagation at the $\Sigma 1$ boundary (Fig. 3a/(ix)). It is notable that the nucleation and propagation of crack were never observed on the specimen surface with high connectivity of the low-Σ boundaries (in the area (I)). On the other hand, the main crack immediately and continuingly advanced along random boundaries in the boundary network with high connectivity of random boundaries (Fig. 3a/(viii–x)). It is confirmed that intergranular crack predominantly and selectively tends to propagate along random boundary network, and never propagates along low-Σ CSL boundaries connecting with this active crack propagation path, resulting in the fatigue crack propagation rate of more than 1.9 μm/cycles which is much higher than that obtained from the area mentioned before, as seen from Fig. 3b.

Let us examine the case of another specimen, similarly tested under cyclic loading. Figure 4a demonstrates the in situ observations on the crack propagation processes obtained from another sulfur-doped nickel specimen (Specimen-2) subjected to cyclic loading. Figure 4b shows the observed change in the local crack propagation rate at different steps of crack propagation in relation to the local nature of grain boundary microstructure for the Specimen-2, shown in Fig. 4a.

The pre-crack (precisely termed "premature-crack") stayed at the triple junction T_1 where $\Sigma 3$ and random boundaries (R_1) interconnected in front of the crack tip (Fig. 4a/(ii)). The crack advanced along the $\Sigma 3$ boundary locating along the extended direction of the propagation of pre-crack (Fig. 4a/(ii)). The crack propagation rate along this $\Sigma 3$ boundary was 1.80×10^{-3} μm/cycle as shown in Fig. 4b. As soon as the crack propagation was stopped on the $\Sigma 3$ boundary, another crack propagation path immediately becomes active along the random boundary (R_1) connecting the triple junction T_1 at the left-hand side. As a result, the branching of crack occurred at the triple junction T_1 (Fig. 4a/(iii)). The crack propagated along the random boundary (R_1) then stopped at the triple junction T_2.

As observed in the case of the Specimen 1, those slip lines which appeared parallel to the surface trace of the $\Sigma 1$ boundary formed in the grain associated with the triple junction T_3. This $\Sigma 1$ boundary cracked accompanying with the formation of a large number of slip lines within nearby grain (Fig. 4a/(iii–iv)). Moreover, the crack propagation along $\Sigma 1$ boundary was immediately directed into the grain interior of one of adjoining grains, resulting in a change in fracture mode, i.e., from intergranular to transgranular fracture, and then finally stopped within the grain interior (Fig. 4a/(v)).

The local propagation rate was $F_i = 5.1 \times 10^{-2}$ μm/cycle for the intergranular crack along the $\Sigma 1$ boundary, and $F_t = 6.9 \times 10^{-3}$ μm/cycle for the transgranular crack in the grain interior, as shown in Fig. 4b. The first and second crack propagation paths joined together by further cyclic loading (Fig. 4a/(vii)). The third crack propagation path along random boundary (R_2) began to operate, after the second crack propagation path became inactive in the grain interior (Fig. 4a/(vi)). The crack immediately advanced along random boundary network in which ten random boundaries were continuously connected to each other (R_2–R_{11}) with no interruption. The intergranular crack propagation rate was accelerated from 5.6×10^{-2} μm/cycle to 0.7 μm/cycle. These results have evidenced that the branching of random boundary connectivity induced by the interaction with low-Σ CSL boundaries is useful and powerful for controlling the crack propagation in sulfur-doped polycrystalline nickel, as previously achieved by the present authors, on the similar principle in order to improve the superplasticity of intrinsically brittle Al–Li alloy through enhanced interaction with newly introduced low-angle ($\Sigma 1$) boundaries by strain rate change during high temperature deformation [40].

Effect of grain boundary microstructure on fracture resistance in sulfur-doped nickel during static bending tests

The present investigation has revealed that the crack propagation process of intergranular brittle fracture in sulfur-doped nickel was predominantly affected by grain boundary microstructure. In particular, the lower connectivity of random boundaries induced the more frequent crack branching and lower crack propagation rate. This section is concerned with SEM observations of fracture surfaces of sulfur-doped nickel specimens with different grain boundary microstructures, in order to confirm the effect of grain boundary connectivity on the fracture mode operating in polycrystalline nickel embrittled by sulfur. The utility of GBE for controlling sulfur segregation-induced embrittlement in polycrystalline nickel is discussed.

(1) Figure 5a and b shows the stress–strain curves obtained by static four-point bending test, taken from the related work recently reported by the present authors [26]. The possible crack propagation processes are schematically shown in Fig. 5c and d with SEM micrographs (Fig. 5e, f) taken from typical fracture surfaces in the fractured specimens with different grain boundary microstructures. First, it should be mentioned briefly how to produce different grain boundary microstructures in nickel specimens.

Type A specimens were prepared by cold rolling to 80 % reduction ratio and subsequent annealing at 923 K for 1.2 ks. These annealed specimens were subjected to

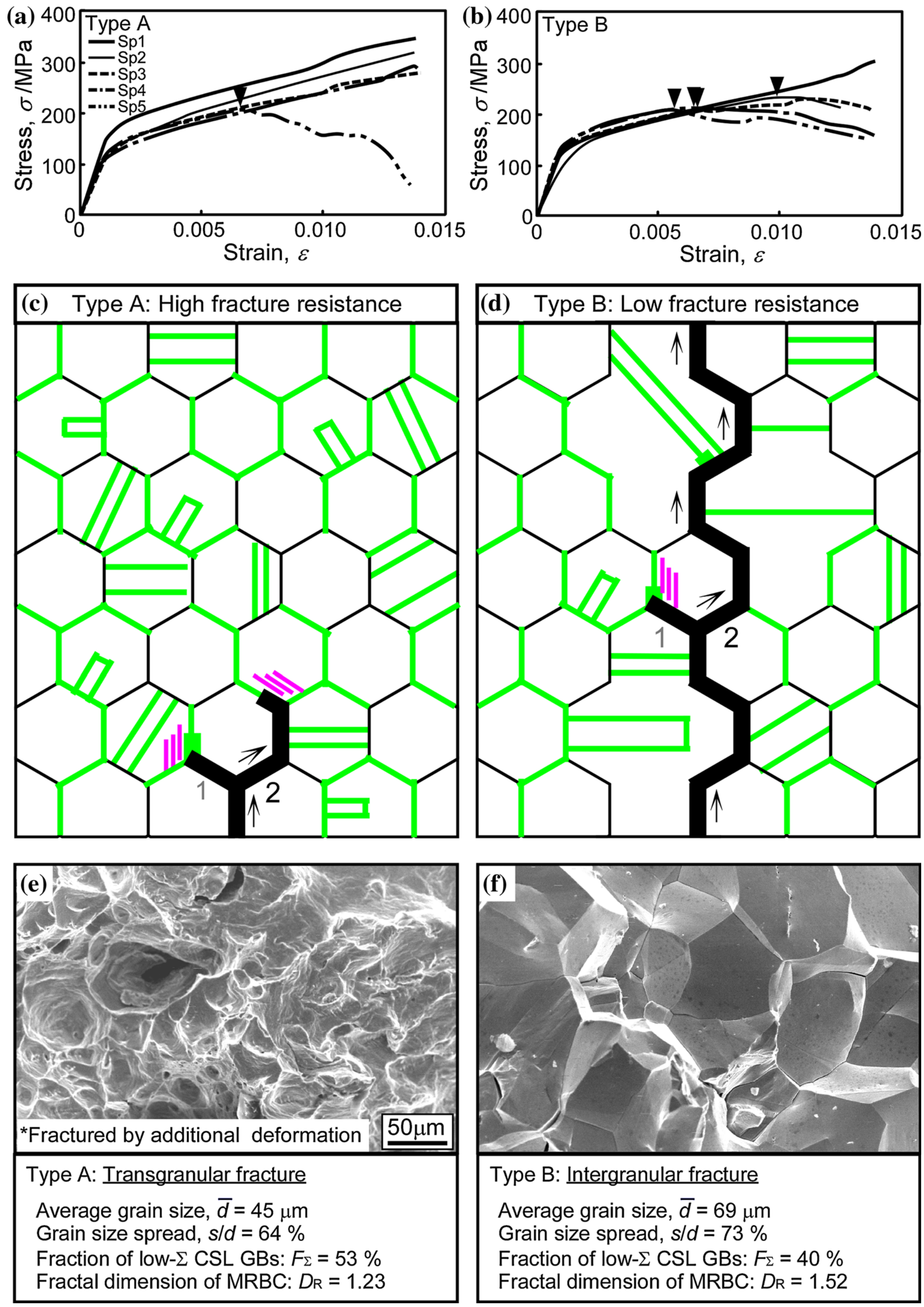

Fig. 5 SEM micrographs of typical fracture surfaces produced by static bending test and schematic illustrations of possible crack propagation processes: **a** and **b** stress strain curves for the Type A, and Type B specimens, with different grain boundary microstructures in sulfur-doped nickel specimens during cyclic loading, **c** and **d** schematic of crack propagation processes, **e** and **f** SEM micrographs of fracture surfaces, respectively

further cold rolling to 5 % reduction ratio and subsequent annealing at 1173 K for 3.6 ks. On the other hand, Type B specimens were obtained by cold rolling to 80 % reduction ratio and subsequent annealing at 923 K for 3.6 ks. These specimens were subjected to further cold rolling to 5 % reduction ratio and subsequent annealing at 1223 K for 1.8 ks. Both Type A and Type B specimens were subjected to sulfur-doping heat treatment. These specimens were enclosed with sulfur powders (0.04 g) in a Pyrex glass tube with 8 mm internal diameter and 70 mm length in a vacuum of 3×10^{-3} Pa and heated at 873 K for 72 h. The average value of sulfur content in these specimens was 290 ppm slightly different between the two types: 270 ppm in Type A specimen, and 310 ppm in Type B specimen. According to Doherty et al. [3], sulfur-induced embrittlement in polycrystalline nickel takes place around room temperature when the sulfur content is increased up to 140 ppm. Moreover, Loier and Boos [4] have reported that embrittlement of polycrystalline occurred when the bulk sulfur concentration ranges from 50 to 200 ppm. Therefore, the sulfur content of both Type A and Type B specimens was considered as being enough for occurrence of sulfur-induced embrittlement in nickel.

Type A specimens had a homogeneous fine-grained structure, a higher fraction of low-Σ CSL boundaries ($F_\Sigma = 53$ %) and a lower fractal dimension of random boundary network with maximum connectivity (maximum random boundary connectivity (MRBC, $D_R = 1.23$) in the specimen. On the other hand, Type B specimens had a heterogeneous grain structure, a lower fraction of low-Σ CSL boundaries ($F_\Sigma = 40$ %) and a higher fractal dimension of MRBC, $D_R = 1.52$. The higher fractal dimension of MRBC can indicate the higher random boundary connectivity.

(2) The stress–strain curves obtained by tensile fracture tests [26] for five different specimens received the same heat treatment are shown in Fig. 5a and b on the top. The arrow heads indicate the position at which a crack seems to nucleate at the bottom of the notch, because the stress irregularity arose on the stress–strain curves. Most of the Type A specimens did not fracture in the range of small bending strain of $\varepsilon = 0.14$, while all of the Type B specimens fractured, when five bending tests were carried out for each type of the studied specimens [26]. The Type A specimens were subjected to excess bending strain until they fractured in order to obtain SEM micrographs of fracture surface.

The crack propagation processes observed in the Type A and Type B specimens are schematically shown Fig. 5c and d. The intergranular crack propagation is inhibited by the frequent interaction with fracture-resistant low-energy/low-Σ CSL boundary in the Type A specimens which had a higher fraction of low-Σ CSL boundaries and a lower fractal dimension of MRBC. As a result, the Type A specimen tends to show a higher fracture resistance. On the other hand, in the case of Type B specimen, the main crack propagates at a higher crack propagation rate without crack branching, due to a lower fraction of low-Σ CSL boundaries and a higher fractal dimension of MRBC, leading to less hindrance of the crack propagation originating from the interaction with low-Σ CSL boundaries.

From SEM micrographs of the fracture surface shown in Fig. 5e and f on the bottom, it is evident that the Type A specimen shows a typical ductile fracture surface accompanying with extensive formation of dimples, while the Type B specimen shows a typical intergranular brittle fracture surface. Accordingly, it is concluded that the fracture mode can drastically change from intergranular brittle to transgranular ductile fracture, resulting in an improvement in the fracture toughness, by increasing the fraction of low-Σ CSL boundaries and decreasing the fractal dimension of MRBC (random boundary connectivity) recently proposed by the present authors [26]. In summary, sulfur-induced intergranular embrittlement of polycrystalline nickel is controlled by the strategy of GBE, based on the introduction of the lower level of random boundary connectivity realized by the introduction of a higher fraction of low-Σ CSL boundaries.

Grain boundary engineering for control of segregation-induced embrittlement

The basic concept of the GBE for controlling segregation-induced embrittlement in polycrystalline material systems is discussed.

The present work based on in situ observations on crack propagation processes has revealed the important role of grain boundary microstructure in fracturing of polycrystalline nickel embrittled by sulfur. Figure 6 schematically shows the crack propagation processes observed in sulfur-doped nickel specimen during cyclic loading. Random boundaries were proved to be the most preferential path of crack propagation. The higher connectivity of random boundaries was found to bring about the higher crack propagation rate in grain boundary network in embrittled

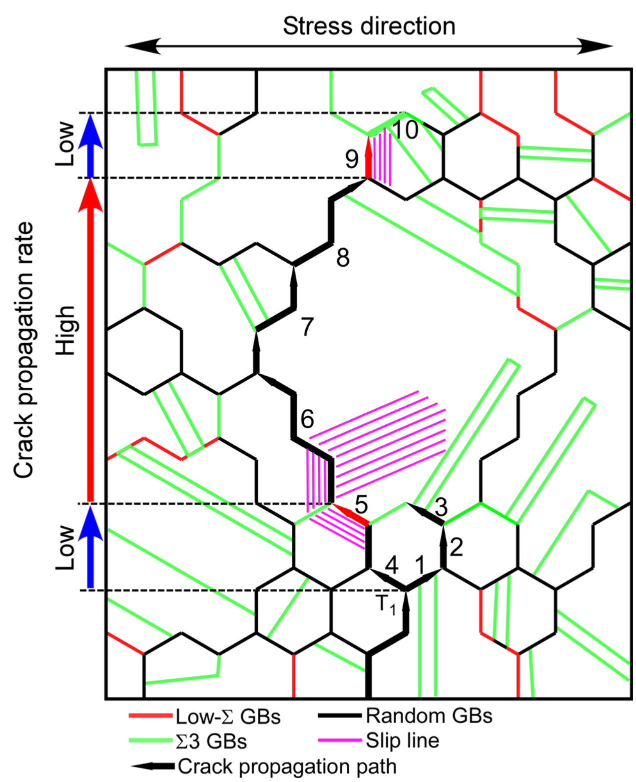

Fig. 6 Schematic illustration of the crack propagation processes in polycrystalline metallic materials with different grain boundary microstructures, leading to the grain boundary engineering for control of segregation-induced embrittlement

polycrystalline nickel. The crack branching occurs at the partly cracked triple junction when the propagating crack along random boundaries is arrested by segregation and fracture-resistant low-Σ CSL boundaries with low energy. When the main propagating crack is arrested, the crack propagation rate tends to locally slow down, due to crack branching resulting in a kind of stress relaxation. The low-Σ boundaries likely fracture only when the grain boundary plane is aligned parallels to the slip direction in adjacent grains. It is concluded that the crack propagation along low-Σ boundaries tends to proceed slowly, resulting in a low crack propagation rate. Accordingly, it is reasonable to expect that the introduction of a higher fraction of low-Σ boundaries and of the lower connectivity of random boundaries can effectively control the dominant occurrence of intergranular fracture along high-energy random boundaries in polycrystalline materials embrittled by detrimental elements.

Conclusions

In situ observations of crack propagation in sulfur-doped polycrystalline nickel specimens were performed in order to clarify possible roles of grain boundary microstructure in crack propagation processes in polycrystalline nickel embrittled by grain boundary segregation of sulfur. The importance of the grain boundary microstructure for controlling segregation-induced intergranular fracture in polycrystalline nickel is discussed based on in situ observations. The main results and conclusions are the following:

(1) The main crack propagates predominantly along random boundaries. The crack propagation rate can be locally accelerated in the region of grain boundary network where random boundaries are more frequently interconnected to each other.

(2) The crack propagation tends to be arrested when the propagating crack reached the triple junction composed of more low-Σ CSL boundaries in the grain boundary network.

(3) The branching of the main propagating crack occurs at the triple junction partly cracked, when the crack propagation is arrested by connecting low-Σ CSL boundaries. The crack propagation rate can be locally affected by occurrence of crack branching, depending on the character of triple junction.

(4) The low-Σ boundaries are generally difficult to fracture, but can fracture only when the trace of the grain boundary is aligned parallel to the slip direction in the adjoining grains. The crack propagation along low-Σ boundaries results in lowering the crack propagation rate or the arrest of crack propagation.

(5) The fracture mode can drastically change from intergranular brittle to transgranular ductile fracture or vice versa, depending on the fraction of low-Σ CSL boundaries and the connectivity of random boundaries. It has been revealed that sulfur-induced embrittlement of polycrystalline nickel can be effectively controlled by GBE through lowering the connectivity of random boundaries by introducing the high fraction of low-Σ CSL boundaries.

References

1. Hondros ED, McLean D (1976) Grain boundary fragility. In: Chadwick GA, Smith DA (eds) Grain boundary structure and properties. Academic Press, London, p 353
2. Kraai DA, Floreen S (1964) The hot ductility of nickel. Trans AIME 230:833
3. Doherty JE, Giamei AF, Kear BH (1974) The importance of grain boundary morphology and cohesion on intergranular strength. Can Metall Quart 13:229
4. Loier C, Boos J-Y (1981) The influence of grain boundary sulfur concentration on the intergranular brittleness of nickel of different purities. Metall Trans 12A:1223
5. Watanabe T, Murakami T, Karashima S (1978) Misorientation dependence of grain boundary segregation. Scripta Metall 12:361
6. Watanabe T, Kitamura S, Karashima S (1980) Grain boundary hardening and segregation in alpha iron-tin alloy. Acta Metall 28:455
7. Lejček P, Paidar V, Adámek J, Hofmann S (1997) Segregation and corrosion behaviour of incommensurate 45°[100] grain boundaries in an Fe–Si alloy: the role of grain boundary plane orientation. Acta Mater 45:3915
8. Lejček P (2010) Grain boundary segregation in metals. Springer-Verlag, Berlin, p 111
9. Floreen S, Westbrook JH (1969) Grain boundary segregation and the grain size dependence of strength of nickel-sulfur alloys. Acta Metall 17:1175
10. Bouchet D, Priester L (1986) Intergranular segregation and crystallographic parameters of grain boundaries in nickel-sulfur system. Scripta Metall 20:961
11. Russell JD, Winter AT (1985) Orientation effects in embrittlement of copper bicrystals by bismuth. Scripta Metall 19:575
12. Kurishita H, Yoshinaga H (1989) Grain boundary fracture in molybdenum. Mater Forum 13:161
13. Tsurekawa S, Tanaka T, Yoshinaga H (1994) Grain boundary structure, energy and strength in molybdenum. Mater Sci Eng A176:341
14. Miura H, Nakata H, Sakai T, Kato M, Mori T (1996) Temperature dependence of embrittlement of Cu [001] tilt boundaries induced by Bi segregation and its correlation with grain-boundary energy, In: Ishida Y, Morita M, Suga T, Ichinose H, Ohashi O, Echigoya J (eds) Interface Science and Materials Interconnection, Proc. of JIMIS-8 and iib'96, The Japan Inst Metals, Sendai, p 249–252
15. Monzen R, Matsuda O, Miura H (2004) Misorientation dependence of intergranular embrittlement of Cu-2.0 wt% Sb bicrystals. Mater Sci Eng A387–389:424
16. Watanabe T, Tsurekawa S, Zhao X, Zuo L (2009) The coming of grain boundary engineering in the 21th century. In: Halder A, Sywas S, Bhattacharjee D (eds) Microstructure and texture in steel and other materials. Springer, London, p 43

17. Watanabe T (2011) Grain boundary engineering: historical perspective and future prospects. J Mater Sci 46:4095. doi:10.1007/s10853-011-5393-z
18. Lin P, Palumbo G, Erb U, Aust KT (1995) Influence of grain boundary character distribution on sensitization and intergranular corrosion of alloy 600. Scripta Metall Mater 33:1387
19. Shimada M, Kokawa H, Wang ZJ, Sato YS, Karibe I (2002) Optimization of grain boundary character distribution for intergranular corrosion resistant 304 stainless steel by twin-induced grain boundary engineering. Acta Mater 50:2331
20. Tsurekawa S, Nakamichi S, Watanabe T (2006) Correlation of grain boundary connectivity with grain boundary character distribution in austenitic stainless steel. Acta Mater 54:3617
21. Michiuchi M, Kokawa H, Wang ZJ, Sato YS, Sakai K (2006) Twin-induced grain boundary engineering for 316 austenitic stainless steel. Acta Mater 54:5179
22. Kokawa H, Shimada M, Michiuchi M, Wang ZJ, Sato YS (2007) Arrest of weld decay in 304 austenitic stainless steel by twin-induced grain boundary engineering. Acta Mater 55:5401
23. Tsurekawa S, Okamoto K, Kawahara K, Watanabe T (2005) The control of grain boundary segregation and segregation-induced brittleness in iron by the application of a magnetic field. J Mater Sci 40:895. doi:10.1007/s10853-005-6507-2
24. Bechtle S, Kumar M, Somerday BP, Launey ME, Ritchie RO (2009) Grain-boundary engineering markedly reduces susceptibility to intergranular hydrogen embrittlement in metallic materials. Acta Mater 57:4148
25. Kobayashi S, Tsurekawa S, Watanabe T, Palumbo G (2010) Grain boundary engineering for control of sulfur segregation-induced embrittlement in ultrafine-grained nickel. Scripta Mater 62:294
26. Kobayashi S, Maruyama T, Tsurekawa S, Watanabe T (2012) Grain boundary engineering based on fractal analysis for control of segregation-induced intergranular brittle fracture in polycrystalline nickel. Acta Mater 60:6200
27. Briant CL (1990) On the chemistry of grain boundary segregation and grain boundary fracture. Metall Trans 21A:2339
28. Mykura H (1980) A checklist of coincidence site lattice relations. In: Balluffi RW (ed) Grain boundary structure and kinetics. ASM, Metals Park, p 445
29. Brandon DG (1966) The structure of high-angle grain boundaries. Acta Metall 14:1479
30. Watanabe T, Fujii H, Oikawa H, Arai KI (1989) Grain boundaries in rapidly solidified and annealed Fe-6.5 mass% Si polycrystalline ribbons with high ductility. Acta Metall 37:941
31. Palumbo G, Aust KT (1992) Special properties of Σ gran boundaries. In: Wolf D, Yip S (eds) Materials interfaces: atomic-level structure and properties chap, 5. Chapman & Hall, London, p 190
32. Watanabe T, Tsurekawa S (1999) The control of brittleness and development of desirable mechanical properties in polycrystalline systems by grain boundary engineering. Acta Mater 47:4171
33. Watanabe T, Tsurekawa S, Kobayashi S, Yamaura S (2005) Structure-dependent grain boundary deformation and fracture at high temperatures. Mater Sci Eng A410–411:140
34. Murr LE (1975) Interfacial phenomena in materials and alloys. Addison-Wesley Publishing Company, Boston, p 146
35. Kobayashi S, Tsurekawa S, Watanabe T (2005) Grain boundary hardening and triple junction hardening in polycrystalline molybdenum. Acta Mater 53:1051
36. Kobayashi S, Tsurekawa S, Watanabe T (2006) Structure-dependent triple junction hardening and intergranular fracture in molybdenum. Phil Mag 86:5419
37. Dingley DJ, Pond RC (1979) On the interaction of crystal dislocations with grain boundaries. Acta Metall 27:667
38. Kokawa H, Watanabe T, Karashima S (1983) Dissociation of lattice dislocations in coincidence boundaries. J Mater Sci 18:1183. doi:10.1007/BF00551988
39. Watanabe T (1984) An approach to grain boundary design for strong and ductile polycrystals. Res Mechanica 11:47
40. Kobayashi S, Yoshimura T, Tsurekawa S, Watanabe T (2003) Grain boundary microstructure-controlled superplasticity in Al–Li–Cu–Mg–Zr alloy. Mater Trans 44:1469